THESIS FOR THE DEGREE OF LICENTIATE OF ENGINEERING

Cryogenic InP High Electron Mobility Transistors in a Magnetic Field

ISABEL HARRYSSON RODRIGUES

Department of Microtechnology and Nanoscience (MC2)

Terahertz and Millimetre Wave Laboratory

CHALMERS UNIVERSITY OF TECHNOLOGY

Gothenburg, Sweden 2019

Cryogenic InP High Electron Mobility Transistors in a Magnetic Field
ISABEL HARRYSSON RODRIGUES

Technical Report MC2-422
ISSN 1652-0769

Terahertz and Millimetre Wave Laboratory
Department of Microtechnology and Nanoscience (MC2)
Chalmers University of Technology
SE-412 96 Gothenburg
Sweden
Telephone: +46 (0)31-772 1000

Chalmers Reproservice
Gothenburg, Sweden 2019

Cryogenic InP High Electron Mobility Transistors in a Magnetic Field
Thesis for the degree of Licentiate of Engineering
ISABEL HARRYSSON RODRIGUES
Department of Microtechnology and Nanoscience (MC2)
Chalmers University of Technology

Abstract

The InGaAs-InAlAs-InP high electron mobility transistor (InP HEMT) is the preferred active device used in a cryogenic low noise amplifier (LNA) for sensitive detection of microwave signals. In this thesis it is demonstrated that the InP HEMT, when placed in a magnetic field, has a strong angular dependence in its output current. This has important implications for the alignment of cryogenic InP HEMT LNAs in microwave detection experiments involving magnetic fields.

InP HEMTs with various gate lengths and gate widths have been fabricated and characterized. The output current for the InP HEMTs was measured in static magnetic fields up to 14 T at different angles in an ambient temperature of 2 K. The results showed that for all InP HEMT devices placed in a perpendicular arrangement, the output current is drastically suppressed. It is shown that the reduction in output current is negligible once placed parallel to the applied field. Furthermore, it was found that the output current strongly depends on the angle between the current direction and the magnetic field. In the investigated device geometry, the output current in the InP HEMT is limited by geometrical magnetoresistance. This was expressed in an output current equation which showed excellent agreement with measured data as a function of angle and magnetic field. Device parameters such as transconductance and on-resistance were found to be significantly affected even at small angles and magnetic fields.

A 0.3-14 GHz cryogenic LNA module based on the same transistor technology used in device experiments was measured in a perpendicular magnetic field at 2 K. The LNA was heavily degraded in gain and average noise temperature already up to 1.5 T. In comparison with previous work reported for GaAs single-heterojunction HEMT LNAs, it is shown here that the effect is much stronger for InP HEMT cryogenic LNAs.

Keywords: InP HEMT, magnetic field, angular dependence, geometrical magnetoresistance, cryogenic, low noise amplifier

Acknowledgements

I am using this opportunity to express my gratitude to everyone who supported me throughout the course of this licentiate.

This work was performed in GigaHertz Centre in a joint research project between Chalmers University of Technology, Low Noise Factory AB, Wasa Millimeter Wave AB, Omnisys Instruments AB and RISE Research Institutes of Sweden. I am grateful to Serguei Cherednichenko and Thilo Bauch for valuable assistance in the noise measurements and the staff involved at LNF for the HEMT and LNA design.

I would like to specifically thank my examiner and main supervisor, Professor Jan Stake and Professor Jan Grahn, for bringing me on board this mission and for supervision of my thesis. I would also like to express my gratitude to my daily supervisors and colleagues: Joel Schleeh, Arsalan Pourkabirian, Giuseppe Moschetti and Eunjung Cha, for their useful comments, remarks and engagement through the learning process of this licentiate thesis. They showed me all the practical aspects of the work, including cleanroom fabrication, laboratory measurements and data analysis. They were always helpful and patiently answered all my questions, and for that I am deeply grateful. Their knowledge, advice and friendly support greatly helped me to carry out this work.

Furthermore I would like to thank all the staff at MC2 and in the cleanroom, for the great environment provided and the pleasant atmosphere.

I would specially like to thank David Niepce, besides from being a good friend, also acting as a mentor and supervisor. This accomplishment would not have been possible without you, thank you! Not to forget, my other friends. Their seemingly endless patience and support during my good and bad moments were of tremendous help throughout these two years and crucial for me during the last weeks of writing!

Finally, I must express my very profound gratitude to my family for providing me with unfailing support and continuous encouragement throughout my years of study and through the process of researching and writing this thesis. I will be forever grateful for your love.

Isabel Harrysson Rodrigues, Gothenburg, October 2019

List of Publications

This thesis is based on the work containted in the following appended papers:

Paper A **Isabel Harrysson Rodrigues**, Arsalan Pourkabirian, Giuseppe Moschetti, Joel Schleeh, Per-Åke Nilsson and Jan Grahn, "Magnetic Influence on Cryogenic InP HEMT DC Characteristics", *Compound Semiconductor Week 2018*, pp. 629-630, 2018.

Paper B **Isabel Harrysson Rodrigues**, David Niepce, Arsalan Pourkabirian, Giuseppe Moschetti, Joel Schleeh, Thilo Bauch, and Jan Grahn, "On the Angular Dependence of InP High Electron Mobility Transistors for Cryogenic Low Noise Amplifiers in a Magnetic Field", *AIP Advances* **9**, 085004, 2019.

Other papers that are outside the scope of this thesis:

* André Dankert, Priyamvada Bhaskar, Dmitrii Khokhriakov, **Isabel Harrysson Rodrigues**, Bogdan Karpiak, M. Venkata Kamalakar, Sophie Charpentier, Ion Garate, and Saroj P. Dash, "Origin and evolution of surface spin current in topological insulators", *PHYSICAL REVIEW B* **97**: 125414, 2018.

* **Isabel Harrysson Rodrigues**, David Niepce, Arsalan Pourkabirian, Giuseppe Moschetti, Joel Schleeh, Thilo Bauch, and Jan Grahn, "Angular Dependence of InP High Electron Mobility Transistors for Cryogenic Low Noise Amplifiers under a magnetic field", *Compound Semiconductor Week* 2019.

* **Isabel Harrysson Rodrigues**, David Niepce, Arsalan Pourkabirian, Giuseppe Moschetti, Joel Schleeh, Thilo Bauch, and Jan Grahn, "On the Angular Dependence of Cryogenic InP HEMTs in a Magnetic Field", WOCSDICE2019*: Workshop on Compound Semiconductor Devices and Integrated Circuits* 2019.

List of Figures

Contents

Chapter 1

Introduction

It is crucial in today's most sensitive detection systems, to read out tiny microwave signals with highest accuracy achievable. A key devices in many of these read out systems is the high electron mobility transistor (HEMT). The HEMT is usually included as an active component of a low-noise amplifier (LNA), which in these type of systems mostly is used at cryogenic temperatures (1-10 K). Some of these systems also rely on the presence of a strong magnetic field, *e.g.* in mass spectrometry [1] or detection of dark matter, *e.g.* in the first results from the HAYSTAC axion search [2],[3]. Magnetic resonance imaging is a another potential application for cryogenic LNAs in a magnetic field and is of immense importance in medical diagnostics [4].

It has long been known that the sensitivity of the cryogenic LNA is affected by the presence of a magnetic field: When aligned perpendicular to the magnetic field, the noise temperature of a cryogenic AlGaAs-GaAs (GaAs) HEMT LNA was shown to be degraded with increasing magnetic field [5][6]. However, reports on the electrical behavior in a magnetic field for the cryogenic InGaAs-InAlAs-InP (InP) HEMT LNA - the standard component used in today's most sensitive microwave receivers - have so far been absent. In this thesis, the InP HEMT cryogenic LNA dependence in a magnetic field has been investigated. It was observed that the gain and noise properties were strongly degraded, even much more than the GaAs HEMT LNA.

The degradation of the InP HEMT cryogenic LNA in a magnetic field can only be understood by measuring the individual InP HEMT at low temperature when exposed to a magnetic field. In this thesis InP HEMT devices have been characterized under applied static magnetic fields of various strengths at various angles, in an ambient temperature of 2 K. Both DC measurements for InP HEMTs and cryogenic noise and gain measurements of the InP HEMT LNA are presented. In the case of perpendicularly applied static magnetic field both the InP HEMT and the InP HEMT LNA were strongly affected. Moreover, in this thesis it is verified that the InP HEMT has an extremely suppressed output drain current as a function of angular orientation with respect to the magnetic field, which has never been shown before. The results presented here demonstrates how the InP HEMT output current is limited by a strong geometrical magnetoresistance effect already at a small angle with respect to the magnetic field. The InP HEMT results explain the strong dependence for the InP HEMT LNA in a magnetic field. This has important implications for the alignment of the cryogenic LNA in a magnetic field for maximum readout sensitivity.

Chapter 2 will provide a background to the HEMT in a magnetic field and some major applications where this knowledge is essential. In Chapter 3, the fabrication of the InP

HEMTs used in the thesis is described. Chapter 3 also covers the special case of the cryogenic InP HEMT in either a perpendicular or parallel magnetic field. In Chapter 4, an InP HEMT cryogenic LNA has been measured in a perpendicular arrangement. The degradation of noise and gain properties are discussed. The final part of the thesis is found in Chapter 5, where the angular dependence of the cryogenic InP HEMT is investigated and the physical mechanism for transistor current limitation in a magnetic field is identified. Finally, Chapter 6 will discuss and conclude the work and provide a future outlook.

Chapter 2

Background

This chapter will provide necessary background information; a description of the main theoretical concepts and related previously published discoveries related to the behaviour of a HEMT in a magnetic field, as well as relevant applications.

2.1 Current Transport in Field Effect Transistors Under a Magnetic Field

It is well known, already since the year 1879, that when using a magnetic field in electric characterization of conducting materials the Hall effect occurs. When a charged particle is traveling with a velocity in a magnetic field it will experience a force, known as the Lorentz Force, which is a result of the Hall effect.

In general, when a semiconductor is placed in a magnetic field the resistivity of the structure increases, mainly depending on the nature of the material and the temperature; this is called physical magnetoresistance effect. The resistance of the semiconductor also increases with increased magnetic field, but depends instead on the geometry of the structure, so called geometric magnetoresistance (gMR). The geometric magnetoresistance is usually the dominating one and increases with higher mobility, since the magnetic field forces the electrons to deviate from their original paths resulting in elevated resistance [7].

Figure 2.1 illustrates a top view of the schematics of a Hall structure and a structure where the gMR can occur. To measure the Hall effect the structure needs to be long rather than wide (L >> W) and the measurement requires at least four contacts. Current runs from contact A to contact B with a contact voltage V_C which will generate a Hall voltage V_H across the sample once a magnetic field is applied in z-led; see Fig. 2.1 (a). In the case of geometric magnetoresistance the sample structure has to be very wide while the length is shorter (L << W); see Fig. 2.1 (b). In the later case the Hall voltage is nearly short circuited due to the long contacts [8][9]. Looking at a HEMT layout with gate length L_g << gate width W_g in a magnetic field according to Fig. 2.1 (c), it is clear that gMR will occur.

Geometric magnetoresistance measurements can be used to investigate both size and material dependent mobilities in nano-scale devices. An example is the channel mobility extraction in transistors [10]. A low-field gMR measurement methodology was used to extract Hall electron mobility μ_H without the influence of series resistance effects. Instead of measuring the magnetic-field-induced resistance change, as in most related publications,

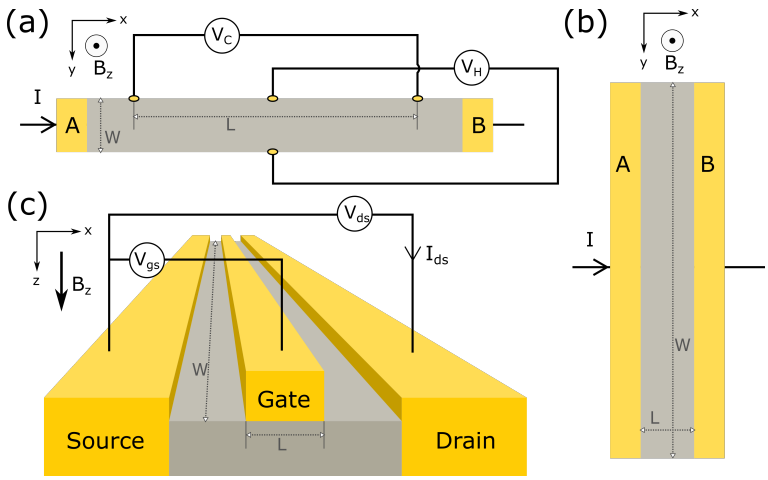

Figure 2.1: Schematic illustration of (a) a Hall measurement with a sample geometry where L >> W (top view), (b) a magnetoresistance measurement of a sample with L << W (top view) and (c) a side view of a HEMT device with $L_g << W_g$, where the B-field is applied in the z-direction.

the investigation in Ref. [10], like in this study, presents the results as a change in drain current I_{ds}.

Another example of mobility extraction using gMR measurements can be found in Ref. [11], where a sub-100 nm n-type metal oxide semiconductor field effect transistor (MOSFET) device was investigated in a magnetic field up to 10 T. The carrier mobility could be measured independently of the carrier concentration and the results were strongly dependent on the geometry of the current flow.

The gMR effect is rather small in low-mobility silicon-based field effect devices [10]. This means that very high magnetic fields are required. In contrast, III-V HEMT devices such as GaAs and InP HEMTs exhibit large gMR already at 1 T [12].

A GaAs HEMT was used in an experiment, published 1997, examining a cryogenic GaAs HEMT LNA in a magnetic field [5]. Their experiment was conducted by measuring the LNA and no data on the actual transistor was shown. The influence of a strong static magnetic field on the DC-characteristics of a HEMT alone has never been reported before. Modern cryogenic InP HEMT based LNAs exhibit four times better performance in noise temperature as well as much higher gain. It is therefore of interest to examine the performance of modern state of the art InP HEMT LNAs under strong magnetic fields.

2.2 Applications

Cryogenic detectors operating in the microwave regime always have a pre-amplifier to pick up the faint signal for subsequent post-amplification, analog-to-digital conversion and signal processing. The position of the pre-amplifier is normally in the cryogenic system as close to the sensor as possible thus minimizing cable losses, thermal variations and to ensure low parasitic capacitance. In the case of investigating biological samples the *Fourier-transform ion cyclotron resonance mass spectroscopy* (FTICRMS) is the preferred choice [1]. In such a system a pre-amplifier is mounted in close proximity of the detector which brings the pre-amplifier close to the superconducting electromagnet *i.e.* the LNA module becomes exposed to a high magnetic field; see Fig. 2.2 from Ref. [1].

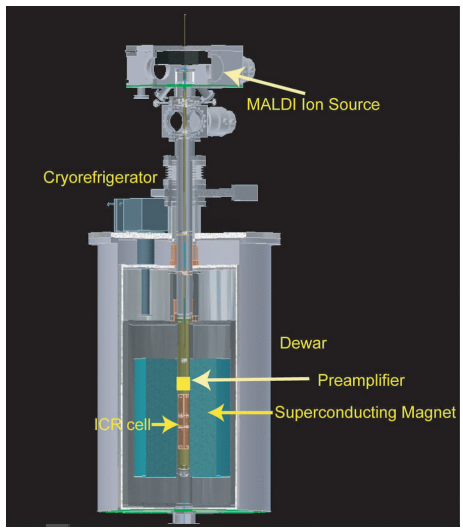

Figure 2.2: Cryogenic FTICRMS cut away view from Ref. [1], where the placement of the LNA is close to the superconducting magnet, as indicated with arrows.

Utilizing cryogenic electronics to increase the signal-to-noise ratio (SNR) within magnetic resonance imaging (MRI) and nuclear magnetic resonance spectroscopy is widely known [**mri26**][13]. Ref. [4] goes through both the design and implementation of cryogenic amplifiers for MRI. In the study the SNR increased by 8% in a 3 T[1] scanner by lowering the ambient temperature of the preamplifier from 300 K to 77 K. Cryogenic LNAs are also used in the study of superconductor analog-to-digital converters for high-resolution MRI in Ref. [14], where a magnetic field up to 4 T were present.

Another interesting application is related to the search for cosmic axions [2]. In the experimental set-up a microwave cavity was used as a detector kept in liquid helium and penetrated with a strong magnetic field. A low-noise microwave receiver was used, which

[1] A clinical MRI system uses a static magnetic field generally ranging from 1.5-7 T.

contained a cryogenic HEMT amplifier coupled to the cavity. The output of the cavity was then amplified with a HEMT amplifier in the GHz range, in an ambient temperature of 3 K and with a magnetic field of 7.5 T present.

2.3 Conclusion

Geometrical magnetoresistance is a phenomenon that can occurs in semiconductor transistors under a magnetic field and has been studied for some time, mainly in measurements for determination of electron mobilities. This physical effect is particular strong in the InP HEMT due to its device layout combined with a high electron mobility at low temperature. As a result, the impact of a magnetic field on a cryogenic LNA is expected to be very strong. The lack of data in the literature for InP HEMTs and corresponding LNAs at low temperature motivated the work reported in this thesis.

Chapter 3

InP HEMTs in Magnetic Field: Parallel and Perpendicular Arrangement

In this chapter, I present the experimental characterization of InP HEMTs when kept in an applied static magnetic field aligned parallel to the device channel as well as perpendicular. The chapter is divided in three main sections, starting with the fabrication process of the InP HEMT devices. The second part covers the experimental set-up and the DC measurements. Finally, an analysis of the measured transistors in parallel versus perpendicular arrangement in a magnetic field is presented.

3.1 Fabrication of InP HEMT Devices

This section describes a generic fabrication process flow for the devices used in this work. A conventional top-down approach have been used, relying on the patterning of thin films via planar lithography and wet etching of an InP based heterostructure. The specific transistors were all fabricated from the same heterostructure; see Fig. 3.1. This heterostructure has been shown to give excellent performance for these type of transistors [15] and were therefore the material of choice for this study. The barrier was thin enough to permit a modulation of the transistor current in the 100 nm L_g technology. At the same time, the barrier was thick enough to suppress gate leakage current which is well-known to be detrimental for the noise figure in the LNA. The channel contained 65% indium which results in a measured Hall mobility of 11 000 cm^2/Vs at 300 K according to the manufacturer. The sheet electron density n_s was $\approx\ 3 \times 10^{12}/cm^{-2}$. The buffer was 5000 nm thick, which was twice the value used in [15]; However, this is judged not to influence the active part of the device. The 4-inch wafers were purchased from an epitaxy foundry, growing the material using molecular beam epitaxy.

Device fabrication started with preparing a substrate, a 17 mm x 17 mm chip, which was diced from a 4-inch wafer with a InGaAs-InAlAs-InP heterostructure, followed by a cleaning process.

The mesa was prepared using laser lithography, chemical wet etching and photoresist stripping. The mesa was verified to have the specified thickness of 80-110 nm using a surface profilometer. The ohmic contacts consisting of an nickel-germanium-gold alloy were prepared by electron-beam lithography, oxide removal and metal deposition, followed by lift-off and rapid thermal annealing.

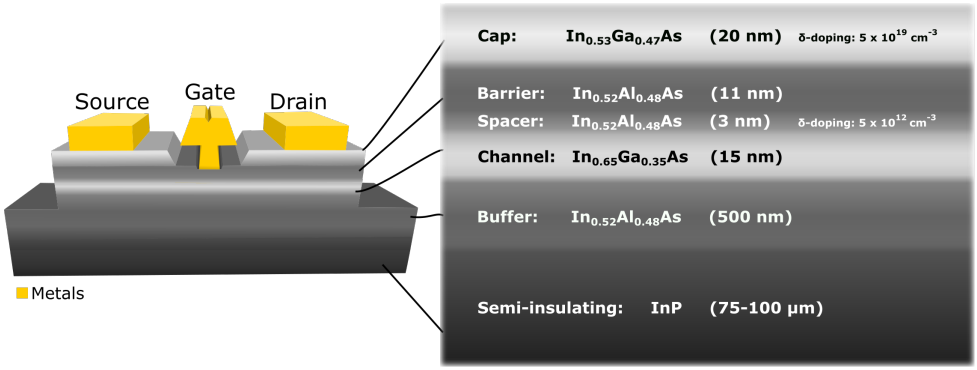

Figure 3.1: InP HEMT investigated in this thesis where the active channel was a 15 nm thin $In_{0.65}Ga_{0.35}As$.

The variation lays in the gate processing. The different gate geometries were determined by which design in the AutoCAD mask that was exposed during the gate electron beam lithography. After the exposure the gate recess was done, as well as oxide removal and metal deposition creating the physical gate after a final lift-off step. The gate material used was titanium, platinum and gold.

To protect the samples and prevent contamination in the sensitive gate area, all samples were passivated with a layer of 60 nm thick Si_3N_4, through thin film deposition. The passivating layer then had to be removed above the contacts, which was done with laser writing, wet etch and photoresist stripping.

Larger pads, for adhesion purposes were then added through laser lithography, oxide removal, metal deposition and the last lift-off.

Both one- and two-finger device layouts were fabricated, with W_g ranging from 20 to 200 μm (2x10 to 2x100 μm) and L_g from 60 to 250 nm. The pictures in Fig. 3.2 shows a scanning electron microscopy image top- and side view of the fabricated device. L_g and W_g are both marked in the image (white arrows).

3.2 Measurement Set-up

The DC-characterization of the InP HEMTs have been carried out in a Quantum Design Physical Property Measurement System (PPMS), using a Keithley 2604B source meter controlled via LabView to bias the samples. The PPMS set-up contains a superconducting magnet enabling measurements up to 14 T in an ambient temperature of 2 K. The transistors were electrically connected through wire bonding to an impedance-matched LC-network (see Fig. 3.3 left image) to stabilize the measurement and avoid oscillations

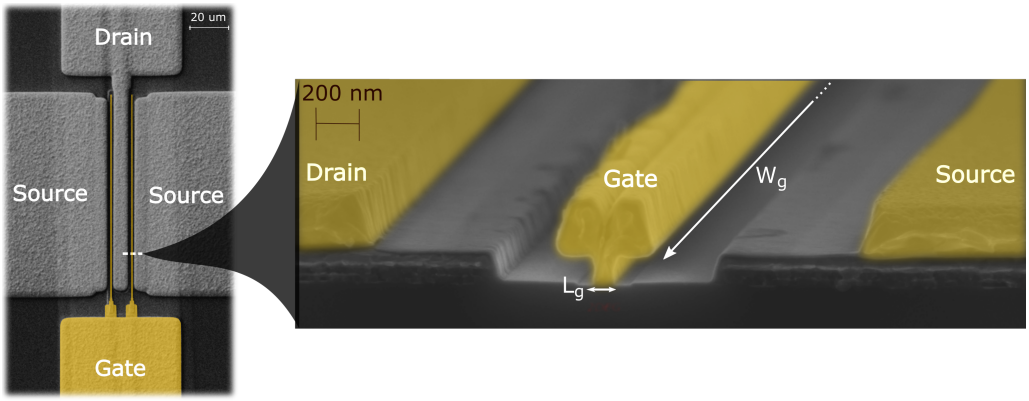

Figure 3.2: Scanning electron microscopy image of a two-finger device and a zoom in on the cross-section of the gate area. Gate area is highlighted in yellow and L_g (100 nm) and W_g (2x100 μm) are indicated with white arrows.

in the output current. The sample was then mounted on a sample holder and placed in the vacuum chamber of the cryostat, where the device channel was oriented either parallel or perpendicular in respect to the applied static magnetic field. The data measured in this set-up were obtained at various occasions over a period of six months, where no fluctuations were observed and the results were reproducible.

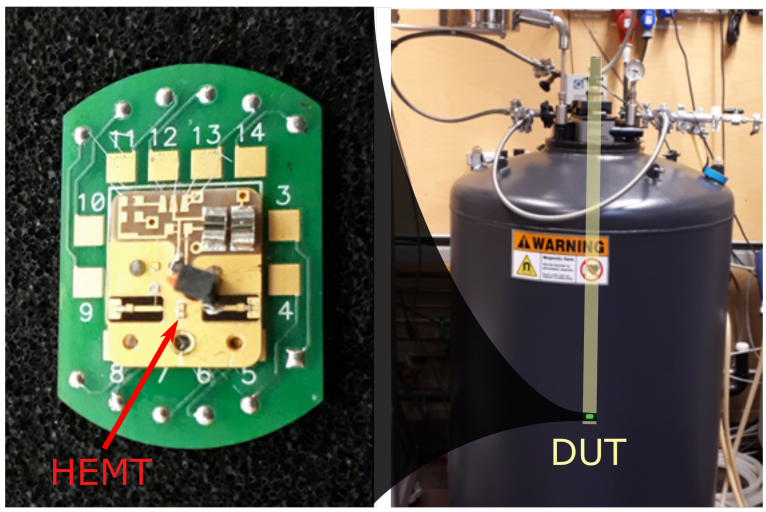

Figure 3.3: Sample holder with an impedance-matched LC-network for measuring the InP HEMTs in the PPMS system (from Paper A).

Both a room-temperature and a cryogenic measurement of the fabricated device was done to confirm the quality of the HEMT [15]. The essential device parameters for a low-noise

transistor were initially measured are presented in Table (3.1). The values obtained are comparable with the ones measures in Ref. [15] and the HEMTs in this study can therefore be considered good enough for further experiments.

Table 3.1: Transistor parameters obtained from a fabricated device with W_g 2x50 μm and L_g 250 nm, measured in room temperature (300 K) and cryogenic temperature (2 K). The transistor was biased with V_{gs} from -0.4 to 0.4 V and V_{gs} from 0 to 1 V.

Parameter	T = 300 K	T = 2 K
$g_{m,max}(V_{gs})$ [S/mm]	1.4	1.9
$g_{ds}(V_{ds,max})$ [S/mm]	0.6	0.8
$R_{on}(V_{ds} = 0.1)$ [Ω mm]	1.11	0.58
$I_{gs,max}(V_{gs})$ [mA/mm]	0.03	0.05
$I_{ds,max}(V_{ds})$ [mA/mm]	428	650

3.3 InP HEMTs in a Perpendicular/Parallel Arrangement

All DC data presented in this chapter are obtained from measurements in respect to the magnetic field done at 2 K on devices with W_g = 2x50 μm and L_g = 100 nm, if not stated other wise.

The InP HEMT was initially tested with the magnetic field oriented perpendicular to the active channel. In Fig. 3.4 (a), the output current is plotted in the absence of a magnetic field. The I-V is very characteristic for an InP HEMT under cryogenic operation [15]. At the current level around the drain voltage V_{ds}=0.4 V a kink behavior is observed and is believed to originate from electron traps in the interface layers of the heterostructure. For the epitaxial structure used here (Fig. 3.1), this is a typical feature at low temperatures. The kink can be suppressed by using an InP etch stopper layer providing better interface, hence reducing traps [16]. Since the sample holder with the LC network, presented in Fig. 3.3, did not provide a perfect 50 Ω impedance-matched environment for the transistor, oscillations occurred for lower I_{ds} showing up as small current jumps. Although these current jumps did not influence the interpretations in this study.

In Fig. 3.4 (b), the measurement was repeated under a perpendicular field of 7 T. It stands clear that I_{ds} is extremely suppressed when exposed to a perpendicular magnetic field. In Fig. 3.4 (c) a strong field of 14 T is applied perpendicular. The effect is extremely strong on the output current: The I_{ds} is reduced by a factor higher than 200 going from 0 to 14 T.

The cryogenic InP HEMT output current was then measured when the active device channel was oriented parallel to the magnetic field. Figure 3.5 (a) shows the maximum source-drain current $I_{ds,max}$, biased at $V_{gs} = 0.4$ V, versus source-drain voltage V_{ds} for applied static magnetic fields ranging from 0 to 14 T. Similar to the plot in Fig. 3.4 (a), a

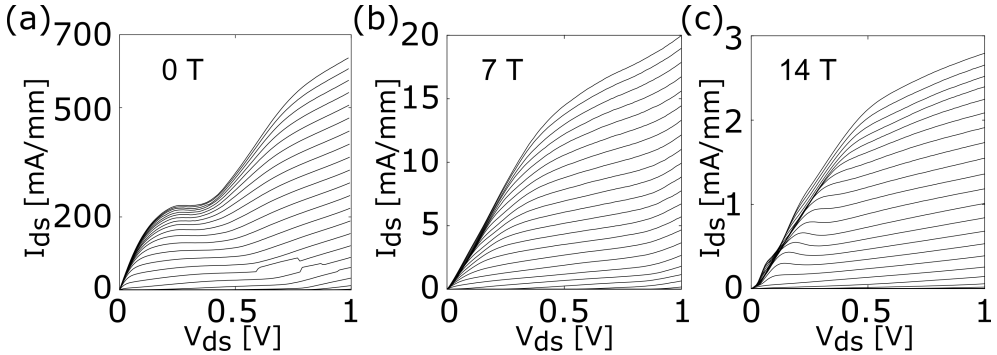

Figure 3.4: I_{ds} versus V_{ds} for the InP HEMT at 2 K oriented perpendicular to a static magnetic field of (a) 0 T, (b) 7 T and (c) 14 T. V_{gs} was varied from -0.4 to 0.4 V in steps of 0.1 V. Note difference in y-axis scale for (a)-(c). L_g = 100 nm, W_g = 2x10 μm. T = 2 K.

current jump around 0.5 V is observed in Fig. 3.5. Again, it is interpreted as a result of mismatch in the impedance of the LC-network. This anomaly will not affect the interpretation of the HEMT electrical behaviour in the experiment. It is concluded that the $I_{ds,max}$ is independent of applied field up to 14 T when oriented parallel to the the magnetic field.

In Fig. 3.5 (b), the $I_{ds,max}$ is plotted for the perpendicular case. In contrast $I_{ds,max}$ is strongly decreased when applying a B-field. It is reduced to almost half its value already at 1 T, and for 10 T there is a 97% reduction in $I_{ds,max}$. The strong suppression of the $I_{ds,max}$ in a magnetic field was also confirmed in Paper A where a one-finger ($W_g = 1x100$ μm and L_g = 100 nm) InP HEMT was measured up to 2 T.

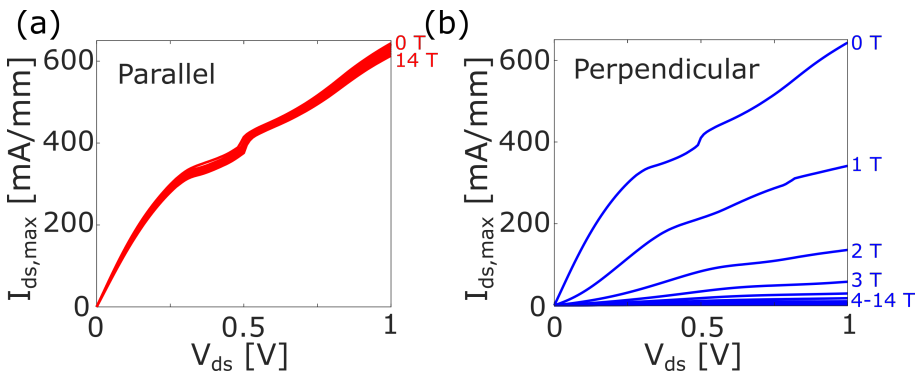

Figure 3.5: (a) and (b) shows $I_{ds,max}$ versus V_{ds} for magnetic fields ranging from 0 T to 14 T at a parallel and perpendicular arrangement respectively. V_{gs} = 0.4 V, T = 2 K.

In Fig. 3.6, the normalized $I_{ds,max}$ is plotted versus the applied B-field. The strong suppression in output current for the perpendicular arrangement is clearly visible and the normalized $I_{ds,max}$ varies as $1/B^2$. In contrast, the effect on I_{ds} from the magnetic

field for the parallel case is negligible. Beyond 10 T a minor reduction can be observed and might be due to a slight mis-orientation of the HEMT in the B-field. $I_{ds,max}$ was measured for both V_{ds}=0.6 and 1.0 V, under saturation, and normalized with respect to zero field. No difference with regard to B can be seen.

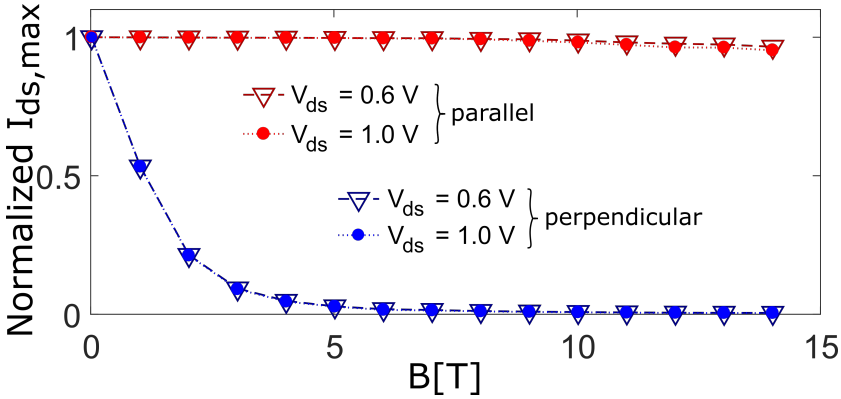

Figure 3.6: Normalized $I_{ds,max}$ versus magnetic field ranging from 0 to 14 T in steps of 1 T with parallel B-field (red) and perpendicular B-field (blue), at V_{gs} = 0.4 V. Values for V_{ds} = 0.6 V (triangle) and 1.0 V (dot) are plotted. T = 2 K. (From Paper B)

The influence of the magnetic field on the InP HEMT output current has large consequences for the on-resistance R_{on} in the device. Fig. 3.7 presents the on-resistance data versus applied magnetic field for the two extreme cases of parallel and perpendicular B-field for a one-finger 1x100 μm device. For the parallel arrangement there is no visible change, but for the perpendicular case R_{on} increases as soon as a magnetic field is applied.

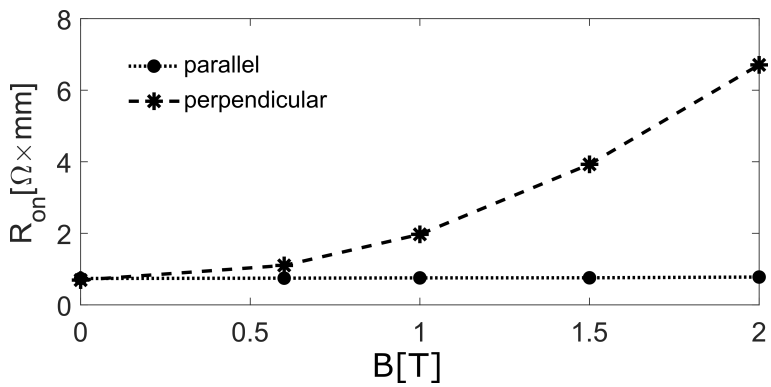

Figure 3.7: R_{on} for the parallel and perpendicular arrangement. V_{ds} = 0 to 0.1 V. T = 2 K.

3.4 Conclusion

It has been shown that the I_{ds} of the cryogenic InP HEMT was heavily reduced when the magnetic field was oriented perpendicular with respect to the HEMT channel. As a consequence, the transistor R_{on} was heavily degraded. In contrast, the device was barely affected when in the parallel arrangement. The observations in this Chapter suggest that a cryogenic InP HEMT LNA is strongly affected in a perpendicular magnetic field arrangement. This is investigated further in Chapter 4.

Chapter 4

InP HEMT Low Noise Amplifier in a Perpendicular Magnetic Field

In Chapter 3, it was found that the InP HEMT output current was heavily affected when the device was positioned perpendicular in a magnetic field at 2 K. In this chapter, an RF characterisation is presented of a cryogenic InP HEMT LNA module at 2 K when the LNA was kept in a perpendicular magnetic field. The chapter is divided in four sections, starting with LNA design, followed by the experimental set-up, then a verification that no ferromagnetic materials were present. Finally, a complete microwave characterization of a full cryogenic LNA module, containing InP HEMTs, is presented.

4.1 LNA Design

The LNA module used in this study was a broadband design ranging from 0.3 to 14 GHz with a gain of 42 dB and average noise temperature of 4.2 K (0.06 dB) [17], at cryogenic conditions and around 6 GHz [18]. This amplifier was mainly chosen for having a wider band width, enabling investigation of several frequencies.

The LNA module contained a monolithic microwave integrated circuit (MMIC) chip consisting of three InP HEMT stages and passive components such as thin film resistors (TFRs) and metal-insulator-metal capacitors (MIM). The MIM cap was a dielectric of Si_3N_4 with a thickness of 150 nm. The MMIC chip had etched via-holes, grounded by a gold plated backside, performed after a substrate thinning [18]. It was then mounted in a gold-plated aluminum module, see Fig. 4.1.

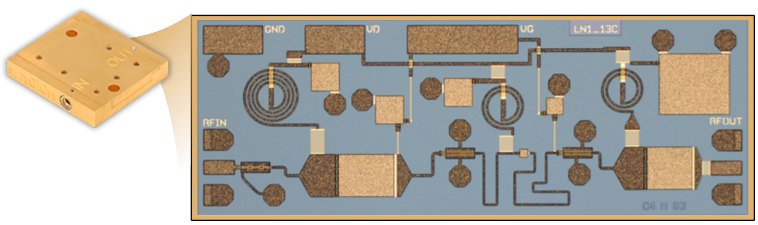

Figure 4.1: Image of the LNA module (size: 19.8 by 20.8 by 3.6 mm [17]) and a photo of the MMIC; a three-stage monolithic microwave integrated circuit with a broadband design ranging from 0.3 to 14 GHz with a gain of 42 dB and average noise temperature of 4.2 K, at cryogenic conditions and around 6 GHz [18].

The transistor technology used in the MMIC was the same as for the discrete InP HEMTs investigated in this thesis. This selected cryogenic wide-band LNA covered typical frequency bands of interest for the detection applications described in Chapter 2.2.

4.2 Verification of Non-Ferromagnetic Materials

The materials in the LNA were all non-ferromagnetic, possibly besides a TFR with a sheet resistance of 50 Ω/□ consisting of an alloy of Nickel (Ni) and Chromium (Cr), where Ni is ferromagnetic. To rule out any influence of the TFR on the device performance in magnetic fields an external TFR were tested.

Verification of non-magnetic properties in the thin film resistor (TFR) was carried out by a regular 4-probe measurement in PPMS at 2 K, using the inbuilt resistance bridge. The measured resistance of the TFR was equal to 58.2 Ω/□ and stayed constant under an applied magnetic field in the interval of 0-2 T. The deviation from 50 Ω/□ was related to process variations in the fabrication, can be negligible and does not influence the result.

No ferromagnetic behaviour was observed, which is consistent with previous studies on non-ferromagnetic metal alloys [19]. Neither the LNA module nor in-going passives exhibited any magnetic-field dependence as verified by additional experiments.

4.3 Microwave Measurements and Set-up

The sensitivity of the cryogenic InP HEMT LNA in a magnetic field was examined using a 10 T superconducting magnet. The LNA was mounted at the center of the magnet on the 2 K stage of an Oxford Instruments Triton 200 dilution refrigerator, see Fig. 4.2 (a). In this arrangement, the LNA module was oriented perpendicular towards the magnetic field. Taking cable loss and an additional attenuator in account, the input signal was attenuated by 27 dB, which was necessary to thermalize the signal going from 300 K to 2 K as well as avoiding saturation of the amplifier.

The device gain was obtained by measuring the S_{21} forward transmission using a ZNB 20 GHz Rohde & Schwarz vector network analyzer (VNA), see schematic set-up in Fig. 4.2 (b). The noise figure was measured using an Agilent N8975A 26.5 GHz noise figure analyzer (NFA), where the noise was generated by an Agilent N4004A SNS, 10 MHz - 18 GHz noise source, see schematic set-up in Fig. 4.2 (c).

By using Joule's first law, the power Gain can be calculated using voltage:

$$Gain(dB) = 10log\left(\frac{\frac{V_{out}^2}{R_{out}}}{\frac{V_{in}^2}{R_{in}}}\right) \tag{4.1}$$

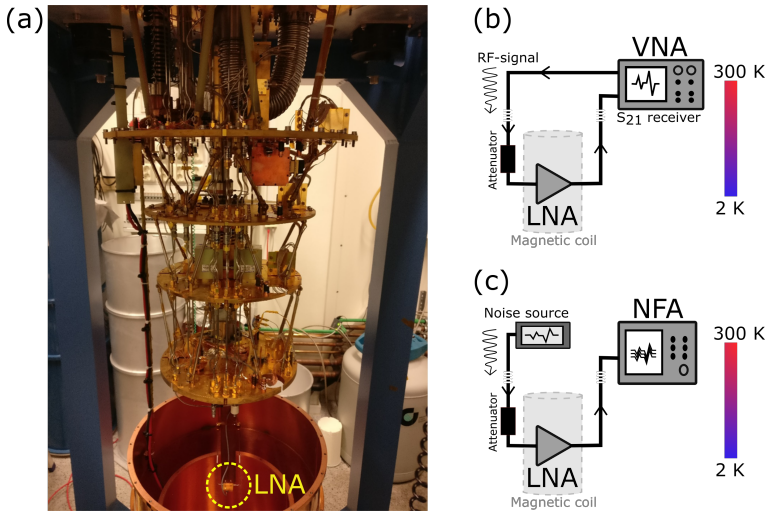

Figure 4.2: (a) RF set-up consisting of an InP HEMT LNA mounted in a Oxford Instruments Triton 200 dilution refrigerator (used at 2 K) with a 10 T superconducting magnet (not visible in the photo). (b) shows a schematic illustration of the gain measurement using a vector network analyzer and (c) shows the noise temperature measurements using a noise figure analyzer and a noise source.

where V_{in} is the input voltage and V_{out} is the output voltage. R_{in} and R_{out} are the input and output impedance, respectively. Here $\frac{V_{out}^2}{V_{in}^2} = G$ is the power gain [20]. In our case R_{out} and R_{in} are equal, which simplifies Eq. (4.1) and the amplifier gain was calculated through the following equation:

$$Gain_{LNA}(dB) = 10log(G * L_{in1} * L_{in2} * L_{out}) \tag{4.2}$$

where L_{in1} is the input loss due to the cables, L_{in2} is the attenuation and L_{out} is the output loss [21].

The noise temperature was calculated using Ref. [22] regarding noise of cascaded components:

$$T_{tot} = T_1 + \frac{T_2}{G_1} + \frac{T_3}{G_1 G_2} + \frac{T_4}{G_1 G_2 G_3} ... \tag{4.3}$$

where T_{tot} represents the noise of the whole system, T_X is the noise temperature for each component, with X being the numbers referring to the cascaded components, $G_X = 1/L_{inX}$ and from Ref. [22] T_{tot} can also be described as:

$$T_{tot} = (F - 1)T \tag{4.4}$$

where F is the noise figure. Using Eq. 4.3 and 4.4, the noise temperature of the LNA, where the LNA is the third cascaded component, can be calculated by solving T_3 in:

$$\frac{(F_3 - 1)T_3}{G_1 G_2} = T_{tot} - (F_1 - 1)T_1 - \frac{(F_2 - 1)T_2}{G_1} - \frac{(F_4 - 1)T_4}{G_1 G_2 G_{LNA}} \tag{4.5}$$

This brings the expression for the noise temperature of the LNA:

$$T_{LNA}(K) = \frac{T - (L_{in1} - 1)T_{in1} - (L_{in2} - 1)T_{in2}L_{in1} - \frac{(L_{out}-1)T_{out}L_{in1}L_{ln2}}{G_{LNA}}}{\frac{L_{in1}}{L_{in2}}} \tag{4.6}$$

Here T is the measured noise of the total system, T_{in1} is the average temperature between the room and the coldest place inside the cryostate which the signal passes on the way in, T_{in2} is the temperature at the LNA and T_{out} is the average temperature between the coldest part of cryostate and the room, which the signal passes on the way out.

4.4 Microwave Characterization of InP HEMT LNA in Perpendicular Magnetic Field

The device characteristics and performance of the InP HEMT LNA were first checked in the absence of any applied field and found to be consistent with specified values [18][17], see Fig. 4.3 for the verification.

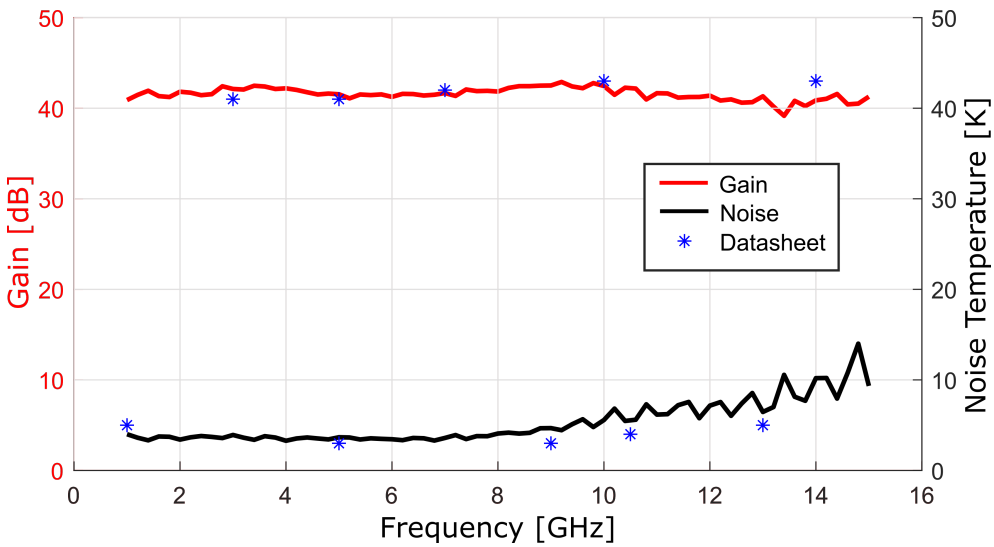

Figure 4.3: Graph showing the measured gain and noise temperature at zero B-field done for verification of accurate experimental set-up. Blue stars (*) are data points taken from the datasheet of the LNA used in this experiment. T =2 K.

In Fig. 4.4 the obtained gain and noise temperature versus frequency of the LNA are presented for the cryogenic InP HEMT LNA at 2 K when exposed to a perpendicular magnetic field up to 1.5 T. Fig. 4.4 (a) shows how the gain is dropping drastically with increased magnetic field. Fig. 4.4 (b) illustrates when the noise temperature increases

with more than 400 % at 1.5 T. It is also observed that the band width becomes degraded with increased B-field.

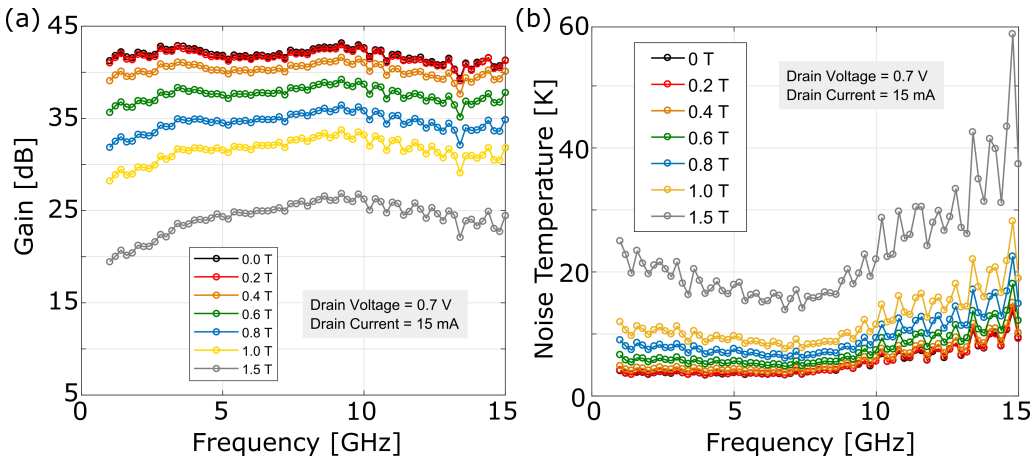

Figure 4.4: Microwave characterisation of a 0.3-14 GHz cryogenic InP HEMT LNA in an ambient temperature of 2 K, measured for fields up to 1.5 T. (a) shows the gain versus frequency, (b) the Noise temperature of the LNA versus frequency.

In Fig. 4.5, the gain and noise temperature versus magnetic field up to 1.5 T at 3, 5 and 8 GHz are presented for the cryogenic InP HEMT LNA. For all three measured frequencies, the gain and average noise temperature of the LNA started to be affected around 0.25 T. In the interval of 0 to 1.5 T, the gain degraded from 42 to 24 dB and the average noise temperature increased from 4 to 18 K, at 5 GHz. For higher fields the gain was so low that post amplification would be needed for further measurements.

4.5 Discussion and Conclusion

In Chapter 3, it was found that the cryogenic InP HEMT rapidly degraded in I_{ds} and R_{on} when subject to a magnetic field perpendicular to the active channel. In this Chapter, the degradation was confirmed also for the InP HEMT cryogenic LNA with respect to gain and noise temperature in the frequency range 0.3 - 14 GHz. The degradation of the LNA properties is very large also at small fields less than 1 T and points to the necessity of avoiding a perpendicular position of the cryogenic LNA in detection of microwave signals.

Comparing the results from this chapter with the earlier study done for a GaAs HEMT LNA in the presence of a magnetic field the effect for an InP HEMT LNA is much stronger [5]. In Fig. 4.6 a plot from Ref. [5] is presenting the noise temperature for a GaAa HEMT LNA under a perpendicular magnetic field and the noise is only increased by a few degrees, in contrast to this study where the average noise temperature increased with approximately 15 degrees. The reasons for this are related to the higher sheet

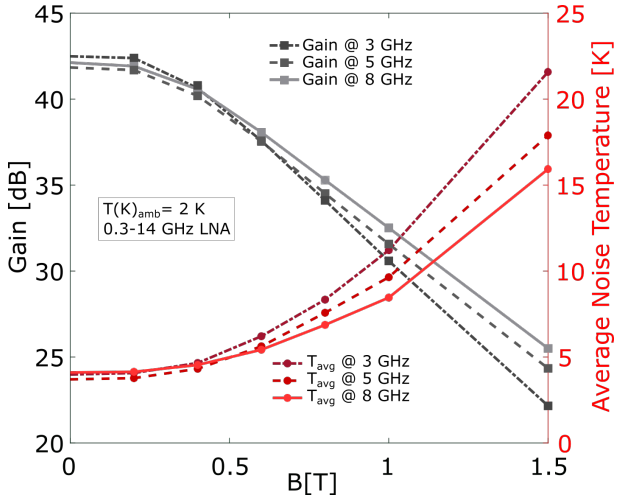

Figure 4.5: Microwave characterisation showing the gain (left axis in black) and noise temperature (right axis in red) versus magnetic field up to 1.5 T, of a 0.3-14 GHz cryogenic InP HEMT LNA in an ambient temperature of 2 K, from Paper B [12].

resistance and the higher electron mobility of the 2DEG in the InP HEMT compared to the cryogenic GaAs HEMT.

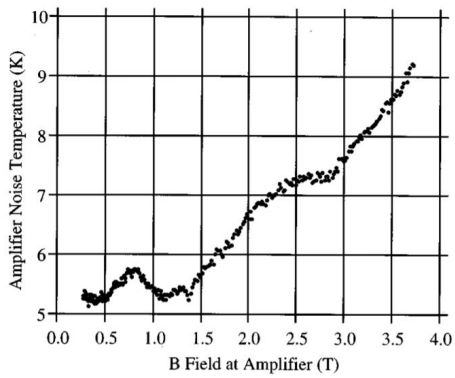

Figure 4.6: Noise temperature for a GaAa HEMT LNA under a perpendicular magnetic field, from Ref. [5].

The results from Chapter 3 suggests that a parallel position of the cryogenic InP HEMT LNA with respect to magnetic field could be unaffected in gain and noise. This could not be investigated in the present setup. The effect of the full angular DC current dependence in a magnetic field could however be measured for the cryogenic InP HEMT in the PPMS. This is the subject for Chapter 5.

Chapter 5

InP HEMTs in Magnetic Field: Angular Dependence

In this chapter, I present a more thorough DC analysis of the InP HEMTs in a magnetic field at various angles in an ambient temperature of 2 K. The chapter is divided in several sections, starting with an angular dependence of the InP HEMT with respect to the angle and the applied static magnetic field B. Here the experimental DC data is plotted in good agreement with a theoretical fit. This chapter also contains device parameters such as transconductance and on-resistance and how they are affected with an applied B-field. All device measurements are performed at 2 K which make the results relevant for the cryogenic InP HEMT LNA.

5.1 InP HEMT Angular Set-up in Magnetic Field

Angular dependence measurements for the InP HEMT were carried out in PPMS at 2 K, with applied static magnetic fields up to 14 T, using a Keithley 2604B source meter controlled via LabView to bias the samples. When measuring the I_{ds} versus B-field characteristics, the sample holder was rotated degree by degree in the range of -45° to 230° enabling accurate detection of small changes in output current in relation to the angle. Fig. 5.1 illustrates the geometry of the DC experiments where the tilt of the sample is marked as θ and the direction of the I_{ds} in the channel is indicated with a thicker arrow. The static magnetic field B was applied in z-led, where $\theta = 0^o$ and $\theta = 90^o$ up till now have been referred to as parallel and perpendicular magnetic field, respectively.

The InP HEMT was first measured for $\theta = 0^o, 30^o, 45^o, 60^o$ and 90^o. In Fig. 5.2, it is observed that the $I_{ds,max}$ is not decreasing linearly with increased B-field. In all investigated cases the effect is clearly stronger at higher fields, which confirms what was observed for $\theta = 90^o$.

After discovering that the InP HEMT was strongly affected also at smaller angles, a more thorough investigation was done. By rotating the transistor in the magnetic field the angular dependence of the cryogenic InP HEMT output current was investigated. Using a step size of 1°, θ was increased from -45^o to 230°. In Fig. 5.3 the I_{ds} is plotted normalized to facilitate comparison within the plot as a function of θ, with an applied static magnetic field up to 10 T. I_{ds} is clearly dependent on θ and this dependence becomes larger with higher magnetic field. Independently of the strength of the applied magnetic field, no change can be observed in I_{ds} once the 2DEG channel of the transistor is aligned 0°

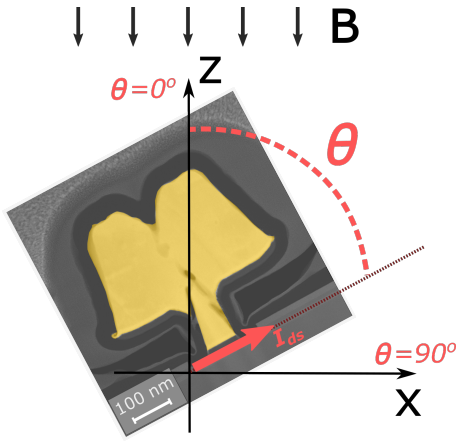

Figure 5.1: A transmission electron microscopy image of the gate illustrating the rotation sweep of the device in a magnetic field, where θ is the angle between the I_{ds} and the magnetic field.

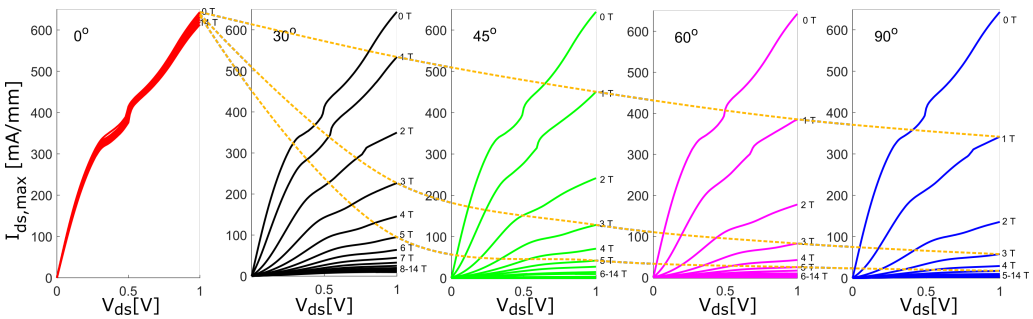

Figure 5.2: Maximum output drain current versus drain voltage at the fix angles of $0^o, 30^o, 45^o, 60^o$ and 90^o for magnetic fields up to 14 T. Yellow striped lines marks the trend of the decreasing $I_{ds,max}$ at 1, 3 and 5 T.

or 180° towards the B-field. For rotations down to 15° there is a significant reduction ($\sim$ 20 %) in I_{ds}, which occurs at an applied field of 3 T. The alignment of the InP HEMT becomes even more crucial when increasing magnetic field and the I_{ds} is reduced by just a few degrees of tilt in θ. It also confirms that the most extreme suppression of the output current occurs at a rotation of 90^o. What is more interesting with Fig. 5.3 is the suppression of I_{ds} being so pronounced (90%) already at $\theta = 30^o$ for the higher fields (8-10 T), again highlighting the large angular dependence of the cryogenic HEMT position in a strong magnetic field.

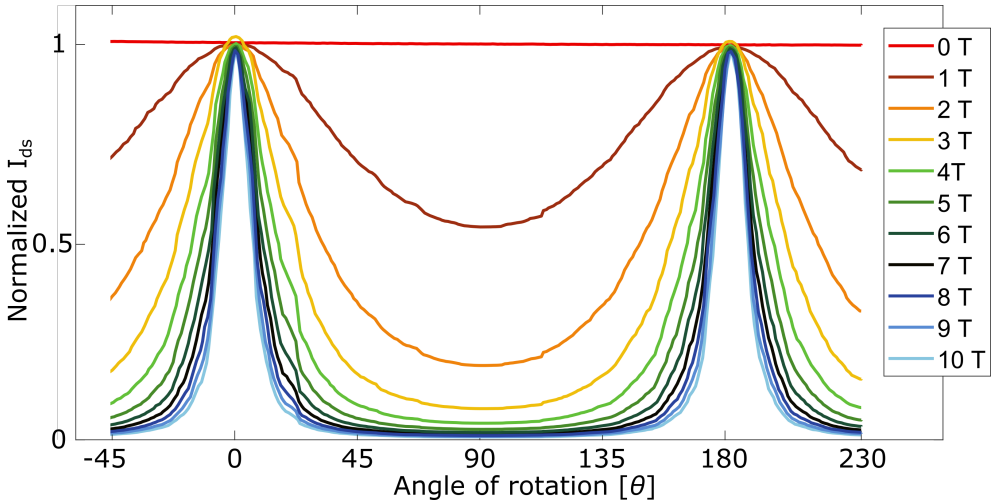

Figure 5.3: Rotation sweep (θ from -45 to 180°) showing the normalized I_{ds} for various externally applied static magnetic fields, 0 to 10 T, at a fix V_{gs} and V_{ds} of 0.4 V in an ambient temperature of 2 K.

5.2 Device Size Dependence in Magnetic Field

Several devices sizes were fabricated and tested in the same experimental conditions (in PPMS at 2 K), only varying the gate geometry. This was done to investigate whether different gate sizes could be correlated with a stronger or weaker geometry dependence, as touched upon in Chapter 2.1. L_g was varied between 60 to 250 nm and W_g was varied between 2x10 to 2x100 μm. Only $\theta = 90^o$ was investigated in this experiment.

In Fig. 5.4 (a) the normalized I_{ds} versus magnetic field is plotted for the samples with varying L_g and (b) presents the equivalent measurements for samples varying W_g. The obtained data shows there is no significant $I_{ds}(B)$ variation in neither L_g nor W_g for $\theta = 90^o$. Even though not experimentally verified, the conclusion drawn from Fig. 5.4 is most probably valid for all θ. Another conclusion is that I_{ds} varies as $1/B^2$ for all curves in Fig. 5.4, which was first observed in Fig. 3.6 for the case $\theta = 90^o$.

5.3 Angular Dependence

In Chapter 2, a background was given on the current transport in a magnetic field for geometries $L << W$. The effect of gMR is profound in the measurements presented in Chapter 3, 4 and 5. This is strongly supported by the $1/B^2$ dependence for I_{ds} in a magnetic field irrespective of device layout as long as $L_g << W_g$. Moreover, the gMR is expected to be large since mobility for InP HEMTs is expected to be very high at cryogenic temperature. The gMR in the active channel will then vary as $1 + \mu^2 B^2$ [10],[23],[8]. Due

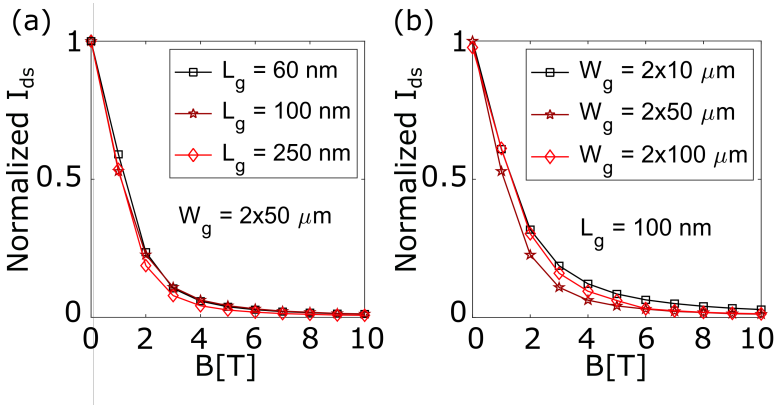

Figure 5.4: Normalized I_{ds} versus magnetic field up to 10 T for InP HEMTs oriented $\theta = 90^{\circ}$ with (a) $L_g = 60$, 100 and 250 nm and (b) $W_g = 2$x10, 2x50 and 2x100 μm. A fix V_{gs} and V_{ds} of 0.4 V were applied in an ambient temperature of 2 K. (From Paper B).

to the geometry and experimental set-up of the experiment (see Fig. 5.1), B is here equal to $B \sin\theta$, which leads to:

$$I_{ds} = \frac{V_{ds}}{R_0(1 + \mu^2 B^2 \sin^2\theta)} \tag{5.1}$$

where R_0 is the channel and access resistance contributions in the measured InP HEMT. When fitting the data from Fig. 5.3 to the derived Eq. (5.1), it shows to be in excellent agreement. In Fig. 5.5, the fitted data is plotted and matched to theory. The angular dependence is symmetrical in I_{ds} around $\theta = 90^{\circ}$. From the fit the parameter R_0 could be extracted and here equals 11 Ω, as well as an extraction of the mobility $\mu = 10,500$ cm^2/Vs, which is what can be expected from this type of measurement [24].

5.4 Transconductance and On-Resistance

Two of the fundamental HEMT parameters for the design of a cryogenic LNA, $g_{m,max}$ and R_{on}, are examined in this section. Fig. 5.6 shows the plotted data for the $g_{m,max}$ as a function of the applied static magnetic field up to 14 T for various angles θ of the cryogenic InP HEMT LNA measured at 2 K. For zero field the $g_{m,max}$ is approximately 1.9 S/mm and decreases drastically as a function of magnetic field already for $\theta = 30^{\circ}$ and above. It is observed that already at 1 T, the $g_{m,max}$ is reduced with 40 % for $\theta = 30^{\circ}$ and 60 % for the extreme case of 90° rotation, also at 1 T.

Compared to Ref. [5], a different $g_{m,max}(B)$ dependence is observed in Fig. 5.6 for $\theta = 90^{o}$. The results in Ref. [5] were extracted indirectly from the cryogenic LNA and therefore, the dependence in Fig. 5.6 is probably more a accurate description of $g_{m,max}(B)$ in the

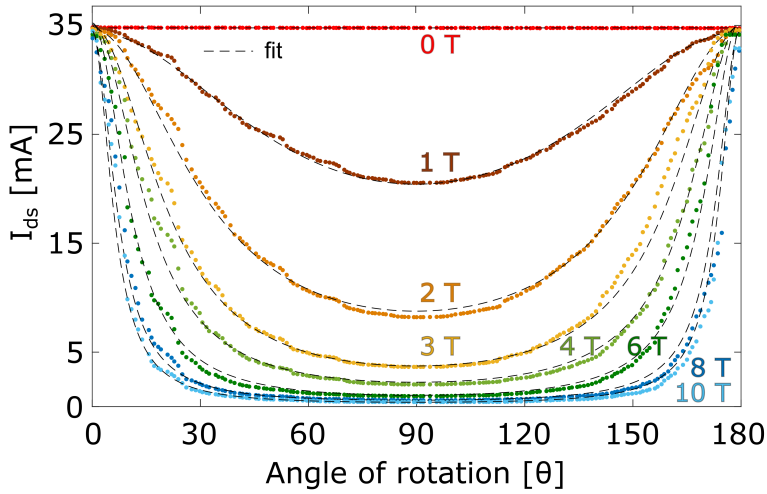

Figure 5.5: Rotation sweep ($0^o < \theta < 180^o$) showing I_{ds} (absolute values) for various externally applied magnetic fields 0, 1, 2, 3, 4, 6, 8 and 10 T at a fix V_{gs} and V_{ds} of 0.4 V in an ambient temperature of 2 K. The dashed lines (black) are fittings of Eq.(5.1) to the experimental data points (colored dots). (From Paper B).

cryogenic HEMT. In Ref. [25], a $g_m(B)$ curve is presented for a JFET[1] perpendicular to the magnetic field at room-temperature. The published curve has more resemblance to the results obtained in Fig. 5.6 for $\theta = 90^o$.

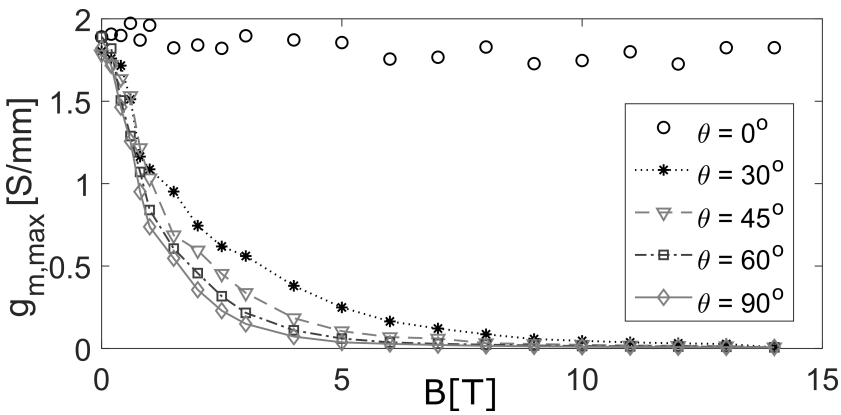

Figure 5.6: The maximum transconductance $g_{m,max}$ as a function of applied magnetic field B[T] up to 14 T for $\theta = 0°$, 30°, 45°, 60° and 90°. Biased at $V_{ds} = 1.0$ V and $V_{gs} = 0.4$ V in an ambient temperature of 2 K.

[1]junction gate field-effect transistor

Fig. 5.7 (a) shows the on-resistance for the InP HEMT as a function of B for various θ, measured at 2 K. When the applied magnetic field is zero R_{on} is approximately 0.7 Ωmm. Regardless of increase in B-field R_{on} does not change for $\theta = 0^{o}$. Although, as expected from the observations done in Fig. 3.5, 3.4 and 3.6, R_{on} increases rapidly with B for $\theta = 90^{o}$. The resistance has already increased with two orders of magnitude at 5 T, when $\theta = 90^{o}$. However, this dependence is also strong at smaller angles, which can be seen for $\theta = 30^{o}$ in Fig. 5.7 (a).

Fig. 5.7 (b) presents R_{on} for $\theta = 90^{o}$. It is confirmed that R_{on} varies as $1 + \mu^2 B^2$ in accordance with Eq. (5.1).

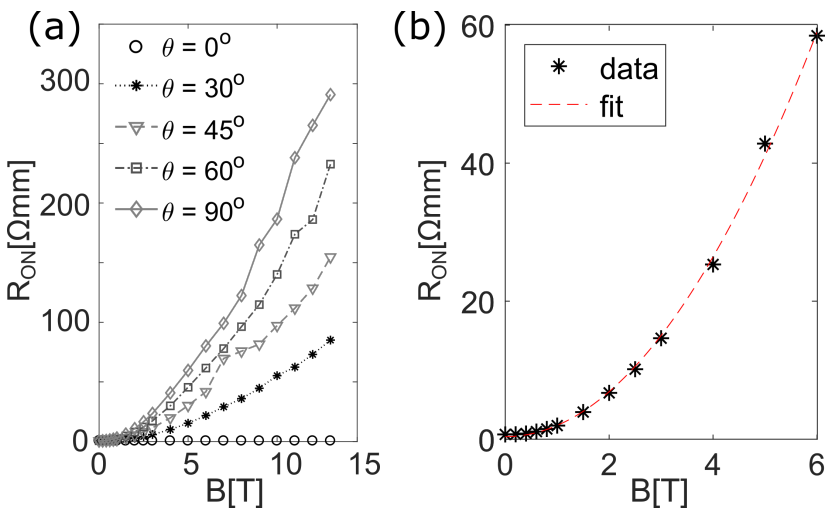

Figure 5.7: (a) R_{on} as a function of applied magnetic field up to 14 T for $\theta = 0^{o}$, 30^{o}, 45^{o}, 60^{o} and 90^{o}. (b) Fit of R_{on} for $\theta = 90^{o}$ using the denominator in Eq. (5.1). T = 2 K, W_g = 2x50 μm, L_g = 100 nm. V_{ds} 0 to 0.1 V and V_{gs} = 0.4 V.

In Fig. 5.7 (a) at higher fields, one can observe what looks like a tendency of oscillations, which brought the attention towards the Shubnikov-de Haas (SdH) effect [9],[24]. To examine these data points further a Fast Fourier Transform (FFT) was done. Unfortunately the amount of experimental data points were limited and the FFT showed to be inconclusive. The large peak observed in Ref. [24] Fig. 3 could be reproduced, but the obtained data was not clean enough to see other oscillations.

5.5 Discussion and Conclusion

In this Chapter, the I_{ds} full angular dependence for the cryogenic InP HEMT has been demonstrated from 0 to 14 T. The limiting current mechanism was identified to be gMR for the full range of investigated θ and B. An I_{ds}-V_{ds} equation captured the θ and B dependence seen in the experiments. It is concluded that this behaviour of the cryogenic InP HEMT has large consequences for $g_{m,max}$ and R_{on}.

Chapter 6

Conclusion and Future Work

In this licentiate thesis, the cryogenic InP HEMT has been investigated in magnetic fields up to 14 T. The angular dependence of the InP HEMT has been studied in detail.

The angle between the applied field and the device channel was crucial for the performance of the transistor. The output current was greatly attenuated not only at a perpendicular arrangement $\theta = 90^{o}$, but also at small θ. The physical reason was identified as gMR occurring for I_{ds} in the cryogenic InP HEMT. This was validated by an accurate fitting of experimental I_{ds} data with an equation describing the gMR as a function of B and θ. Furthermore, the strong influence from θ for the transistor parameters $g_{m,max}$ and R_{on} have been shown, when the cryogenic InP HEMT is exposed to a magnetic field.

The observed large effects of the InP HEMT figures-of-merit such as $g_{m,max}$ and R_{on} leads to the conclusion that a cryogenic InP HEMT LNA will be strongly degraded in RF properties. This was confirmed by testing a wideband InP HEMT cryogenic LNA in a perpendicular magnetic field.

The results from this thesis strongly suggests that even a minor mis-orientation (with a few degrees) of the cryogenic InP HEMT LNA will have large negative effects on amplifier sensitivity in a magnetic environment which is detrimental to read-out signal.

It is evident that today's InP HEMTs are very sensible to mis-alignments under in a magnetic field and the output current is drastically affected already at small angles. While, in their pioneering work on gMR by Jervis and Johnson [22], it was claimed that "Although the magnetic field should be parallel to the contacts, this alignment is not critical". Even though this research was performed a long time ago on other samples and magnetic field strengths, the statement is certainly not valid for the results in this thesis: Indeed, the alignment of the cryogenic InP HEMT is here proven to be extremely critical with respect to the magnetic field.

6.1 Outlook

Shifting the focus from measurements to the design of the HEMT, other geometries could be investigated to examine any variation in the sensitivity, without jeopardising the standard performance of the HEMT. Investigations regarding the case when L is approaching W and the gMR no longer is the dominant effect could be done, examining if and when the $1/B^2$ dependence is wearing off.

Going from device to module, the LNA is worth pursuing. It has been shown to be extremely sensitive to magnetic fields in a perpendicular arrangement and expected to be unaffected once aligned parallel, but it is still unknown how sensitive the InP HEMT LNA would be once tilted a few degrees. Therefore, a more thorough investigation of the angle dependence of the InP HEMT LNA module should be investigated. A wider range of frequencies could also be tested, covering more application areas.

Appendix A

Abundant Material

Here are some additional plots of abundant measurement data, to emphasise and illustrate the unchanged behaviour when varying the gate geometry; see Fig. A.1 (a), (b) and (c).

Fig. A.1 (d) shows measurements done on the same device only varying the ambient temperature from 300 K to 2 K. The angular dependence observed is the same, only the resistance changes, which is expected at lower temperatures.

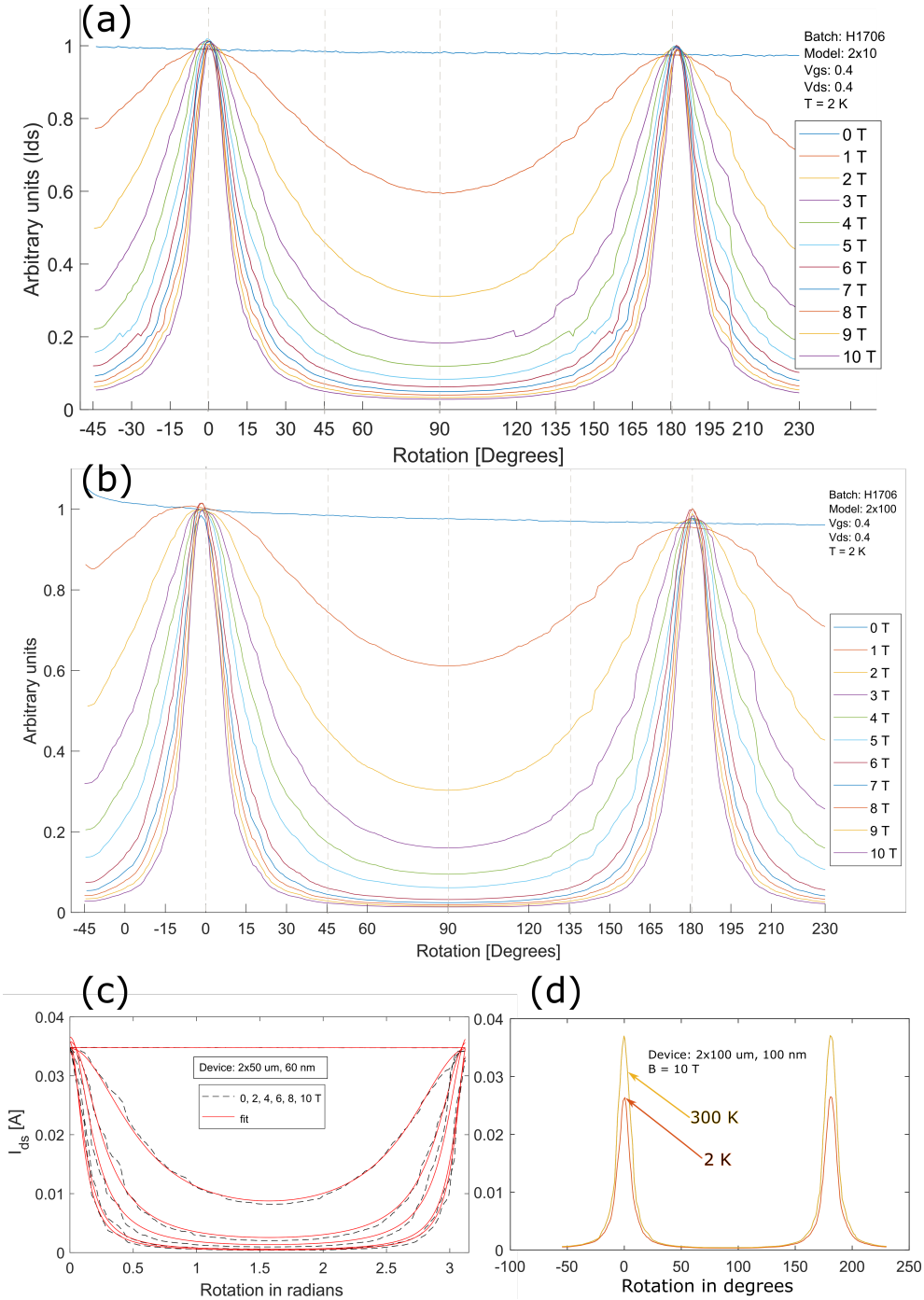

Figure A.1: Rotation sweeps for devices with various gate geometry. (a) $W_g = 2 \times 10\mu m$ (b) $W_g = 2 \times 100\mu m$ and (c) $L_g = 60\ nm$ with fit applied. (d) shows a measurements done in room temperature versus 2 K.

References

1. Mathur, R., Knepper, R. W. & O'Connor, P. B. "A Low-Noise Broadband Cryogenic Preamplifier Operated in a High-Field Superconducting Magnet". *IEEE Transactions on Applied Superconductivity* **18,** 1781–1789 (Dec. 2008).

2. Hagmann, C., Sikivie, P., Sullivan, N. S. & Tanner, D. B. "Results from a search for cosmic axions". *Phys. Rev. D* **42,** 1297–1300 (4 Aug. 1990).

3. Brubaker, B. M. *arXiv e-prints* (Jan. 2018).

4. Johansen, D. H. *et al.* "Cryogenic Preamplifiers for Magnetic Resonance Imaging". *IEEE Transactions on Biomedical Circuits and Systems* **12,** 202–210 (2018).

5. Daw, E. & Bradley, R. F. "Effect of high magnetic fields on the noise temperature of a heterostructure field-effect transistor low-noise amplifier". *Journal of Applied Physics* **82(4),** 1925–1929 (1997).

6. Bradley, R. "Cryogenic, low-noise, balanced amplifiers for the 300–1200 MHz band using heterostructure field-effect transistors". *Nuclear Physics B - Proceedings Supplements* **72.** Proceedings of the 5th IFT Workshop on Axions, 137–144 (1999).

7. Schroder, D. K. *Semiconductor material and device characterization.* (IEEE Press, 2006).

8. Look, D. C. "Review of Hall Effect and Magnetoresistance Measurements in GaAs Materials and Devices". **137,** 260–266 (1990).

9. Chang, C., Fetterman, H. R. & Viswanathan, C. R. "The characterization of high electron mobility transistors using Shubnikov–de Haas oscillations and geometrical magnetoresistance measurements". *Journal of Applied Physics* **66,** 928–936 (1989).

10. Campbell, J. P. *et al.* "Geometric Magnetoresistance Mobility Extraction in Highly Scaled Transistors". **32,** 2010–2012 (2011).

11. Meziani, Y. M. *et al.* "Magnetoresistance characterization of nanometer Si metal-oxide-semiconductor transistors". *Journal of Applied Physics* **96,** 5761–5765 (2004).

12. Harrysson Rodrigues, I. *et al.* "On the angular dependence of InP high electron mobility transistors for cryogenic low noise amplifiers in a magnetic field". *AIP Advances* **9,** 085004 (2019).

13. Fontana, G. *et al.* "Improved sensitivity of planar microwave based RF-SQUIDs using a cryogenic HEMT preamplifier". *IEEE Transactions on Applied Superconductivity* **3,** 1820–1823 (Mar. 1993).

14. Radparvar, M. *et al.* “Superconductor Analog-to-Digital Converter for High-Resolution Magnetic Resonance Imaging”. *IEEE Transactions on Applied Superconductivity* **25,** 1–5 (June 2015).

15. Schleeh, J. *et al. IEEE Electron Device Letters* **33,** 664–666 (May 2012).

16. Rodilla, H., Schleeh, J., Nilsson, P. & Grahn, J. “Cryogenic Kink Effect in InP pHEMTs: A Pulsed Measurements Study”. *IEEE Transactions on Electron Devices* **62,** 532–537 (Feb. 2015).

17. Low Noise Factory AB. *0.3-14 GHz Cryogenic Low Noise Amplifier.* datasheet. Low Noise Factory (LNF-LNC0.3_14SA, July 2018).

18. Schleeh, J., Wadefalk, N., Nilsson, P., Starski, J. P. & Grahn, J. *IEEE Transactions on Microwave Theory and Techniques* **61,** 871–877 (Feb. 2013).

19. Abrecht, M., Adare, A. & Ekin, J. W. “Magnetization and magnetoresistance of common alloy wires used in cryogenic instrumentation”. *Review of Scientific Instruments* **78,** 046104 (2007).

20. Gonzalez, G. *Microwave transistor amplifiers : analysis and design.* (Prentice Hall, 1997).

21. Collin, R. E. *Foundations for Microwave Engineering.* (Wiley-IEEE Press, 2001).

22. Pozar, D. M. *Microwave and RF wireless systems.* (Wiley, 2001).

23. Jervis, T. & Johnson, E. “Geometrical magnetoresistance and hall mobility in gunn effect devices”. *Solid-State Electronics* **13,** 181–189 (1970).

24. Matheoud, A. V., Sahin Solmaz, N. & Boero, G. “A Low-Power Microwave HEMT *LC* Oscillator Operating Down to 1.4 K”. *IEEE Transactions on Microwave Theory and Techniques* **67,** 2782–2792 (July 2019).

25. Bodart, J. R. *et al.* “The effect of high magnetic fields on junction field effect transistor device performance”. *Review of Scientific Instruments* **69,** 319–320 (1998).